Relation Between a Singly-Periodic Roughness Geometry and Spatio-Temporal Turbulence Characteristics

Jonathan P. Morgan

Graduate Aerospace Laboratories
California Institute of Technology
1200 East California Blvd
Pasadena, CA, 91125, USA
jmorgan@caltech.edu

Beverley J. McKeon

Graduate Aerospace Laboratories
California Institute of Technology
1200 East California Blvd
Pasadena, CA, 91125, USA
mckeon@caltech.edu

ABSTRACT

A stationary, spatially-varying disturbance in the mean velocity field of a turbulent boundary layer is created by introducing a singly-periodic roughness of large wavelength. The spatial inhomogeneity extends through the whole boundary layer as a result of the large length scales introduced by the roughness. The roughness also creates spatial inhomogeneity in the power spectrum of the flow, particularly at Taylor-transformed wavelengths corresponding to the roughness wavelength. Spatial inhomogeneity in the time-averaged velocity field and in the power spectrum reveals a phase-organizing effect of the mean velocity field on triadically-consistent pairs of traveling waves. Implications for real-world roughness are discussed.

INTRODUCTION

Turbulent boundary layers are a pervasive phenomenon throughout nature and industry, with applications to aviation, climate, and the environment. Rough-wall turbulent boundary layers in particular contribute a large percentage of the drag and therefore energy costs for ships, air vehicles, and industrial pipelines. An understanding of rough-wall-bounded flow physics allowing effective drag reduction through flow control has the potential to save billions of dollars a year in fuel costs worldwide. While a canonical fully-developed smooth-wall boundary layer has a single parameter in the Reynolds number, the characteristics of a rough-wall boundary layer depend also on the potentially infinite number of geometrical parameters which describe the surface roughness. The infinite possible parameter space cannot be fully explored by simulations and experiments, posing a problem for design engineers and analysts who would like a cheap method to know the effects of a particular arbitrary roughness. A better understanding of the fundamental physics which connect the geometry of the roughness to the behavior of the boundary layer could speed design and possibly reduce drag by narrowing the parameter space and improving simulations.

Experiments and Simulations on Idealized Roughnesses

With such great potential rewards, there has been intense study to determine the relation between a roughness geometry and its effect on the boundary layer. MacDonald *et al.* (2016) have shown that a direct numerical simulation in a sinusoidally-rough channel with very limited spanwise domain of a few roughness wavelengths can give a sufficient wall boundary condition to a full-domain, lower resolution DNS to accurately reproduce the exact flow. This method is more efficient than performing a full DNS with high enough resolution to resolve the roughness. This indicates that the eddies which provide the physical link between roughness geometry and the physics of the roughness sublayer have a size on the order of the roughness wavelength. Flack & Schultz (2014) examined the

statistical moments of roughness topology to find correlations between roughness distribution and alterations in the mean velocity profile. By using proper orthogonal decomposition to extract a low-order representation of a real-world roughness, Mejia-Alvarez & Christensen (2010) explored the importance of individual roughness scales to flow physics. They found that a 3D-printed low-order roughness constructed from the fifteen most amplified proper orthogonal decomposition (POD) modes accurately reproduced the drag characteristics of the full roughness in channel flow, despite the absence of the majority of the scales of the full roughness. The flow physics of the full roughness boundary layer was affected by only the key subset of geometric scales isolated in the experiment. The present work proceeds in the opposite direction, by creating a simple, singly-periodic roughness to observe the effect on the flow of a single large roughness scale.

Amplitude Modulation of Small-Scale Turbulence by Large-Scale Structures

Large scale velocity disturbances are known to correlate with small-scale flow physics in canonical smooth-wall flows. Bandyopadhyay & Hussain (1984) found a correlation between the low-frequency (large-scale) content of a streamwise velocity signal and the envelope of the high-frequency (small-scale) content, varying systematically across shear flows and boundary layers in a consistent way. The correlation was quantified by Mathis *et al.* (2009) with the amplitude modulation correlation coefficient R. Under this approach, the large scale velocity fluctuations u_L and small scale fluctuations u_S are separated from the full velocity time series by a filter and considered as independent signals. The envelope of the small scale fluctuations E is calculated as a function of time using the Hilbert transform. The envelope is then filtered to isolate large-scale modulation of the envelope, resulting in the time series E_L. This quantity is then compared to the large scale fluctuations using the temporal correlation coefficient to yield the amplitude-modulation correlation coefficient, R in Equation 1, with a bar indicating a time average. In smooth-wall flows, R attains a maximum in the viscous region, dips below zero in the log region, and attains a minimum in the wake region.

$$R = \overline{u_L E_L} / \left(\sqrt{\overline{u_L^2}} \sqrt{\overline{E_L^2}} \right) \qquad (1)$$

Duvvuri & McKeon (2015) showed the amplitude modulation coefficient R to be a measure of average phase for pairs of small turbulent scales which are triadically consistent with the large scales. Furthermore, the authors probed the phase organization between scales by perturbing a boundary layer with an oscillating transverse rib, introducing a spanwise-constant synthetic large-scale mode into

the flow. A new correlation coefficient, analogous to R above, was defined as in Equation 2, with tildes here referring to a phase average with a period equal to the oscillation period of the rib.

$$\Psi = \overline{\tilde{u}\tilde{u_S^2}} / \left(\sqrt{\overline{\tilde{u}^2}} \sqrt{\overline{\tilde{u_S^2}^2}} \right) \qquad (2)$$

The quantity Ψ was found to be near one close to the wall, indicating perfect correlation. Around the critical layer of the flow (the wall-normal location at which the mean velocity is equal to the convection speed of the synthetic mode), Ψ changes abruptly to nearly -1 for nearly a decade of height, indicating perfect anti-correlation. Ψ then begins to increase toward 1 at the edge of the boundary layer. In this way, it is shown that a synthetic mode organizes the phases of triadically-consistent scales in a quasi-deterministic manner.

LARGE-SCALE SINGLY PERIODIC ROUGHNESS

The present work aims to explore the relationship between roughness geometry and boundary layer physics with an idealized sinusoidal roughness. The sinusoidal roughness alters the boundary condition of the flow in a simple way, which creates a static inhomogeneous mean velocity field with simple spatial-spectral composition in the flow. This mean velocity field interacts nonlinearly with the turbulence of the boundary layer at a range of other scales to alter the mean quantities of the flow. Due to the comparable wall-parallel wavelengths compared to the boundary layer thickness, the effects of the roughness extend through much of the boundary layer, and hot wire anemometry can be used to measure the spatial variation in mean quantities, statistics, and power spectra required to trace the effects of the roughness.

Roughness Geometry

A roughness surface defined by a height function $h(x,z)$, consisting of a single streamwise-varying Fourier mode with amplitude a and wavelength λ_x added to a single spanwise-varying Fourier mode with amplitude a and wavelength λ_z, as in Equation 3, was 3D-printed.

$$h(x,z) = a\cos(2\pi x/\lambda_x) + a\cos(2\pi z/\lambda_z) \qquad (3)$$

The $y = 0$ plane is therefore located at the average roughness height. The wavelengths $\lambda_x^+ = 950$ and $\lambda_z^+ = 475$ (20mm and 10mm respectively) were chosen as a compromise between matching the observed peak of the velocity power spectrum and allowing hot-wire accessibility between peaks. The amplitude of both modes of the roughness was chosen to be 9 viscous units, physically $182\mu m$. This allowed the roughness amplitude to remain small compared to boundary layer thickness δ while also accommodating the resolution of the 3D-printer. The 3D-printed surface was mounted into an existing test section in the Merrill wind tunnel at Caltech, covering a span of 597mm and a length of 1605mm. Hot-wire measurements were taken 1000mm downstream of the leading edge of the roughness.

Run Conditions

Experiments were performed in the Merrill wind tunnel at Caltech. The test section of the wind tunnel measures 2440mm in the streamwise direction, with a square cross-section that measures 610mm on each edge. The boundary layers were developed over an acrylic plate which spans the width of the wind tunnel. The boundary layers are tripped near the parabolic leading edge, with hot-wire measurement taking place 1250mm downstream of the trip. The pressure gradient is controlled by a deformable ceiling, which is adjustable at ten points along the test section. Freestream velocity U_∞ and velocity profiles were measured with hot-wire anemometry. 99% boundary layer thickness δ was calculated directly from the spatially-averaged velocity profile. Friction velocity u_τ was determined by a single iteration of the modified Clauser method. Rough-wall measurements were taken at a Reynolds number of $Re_\delta = 26000$, $Re_\tau = 1200$, while smooth-wall measurements were taken at $Re_\delta = 29000$, $Re_\tau = 1100$. The acceleration parameter $K = \frac{\nu}{4U_\infty^3\rho}\frac{dp}{dx}$, as defined by De Graaff & Eaton (2000), was of the order 1×10^{-8} for both the smooth and the rough case, indicating a nominal zero-pressure gradient turbulent boundary layer.

Hot-Wire Measurements

A hot-wire probe was mounted on a post fixed below the test surface and extended through a port cut into the roughness and test surface. A traverse allowed measurements at multiple wall-normal distances during a single test run, and the hot wire probe was adjusted between experiments in the streamwise and spanwise directions to alter the position of the measurement volume. Eight traverses were made over a single period of roughness, in a grid that spanned four stations in the streamwise direction and two stations in the spanwise direction. For each station and y-location, 100s of streamwise velocity data were recorded, equal to 74,000 eddy turnover times (δ/U_∞).

All measurements shown in this paper were taken at wall-normal positions greater than the maximum roughness height ($y > 2a$). Flow reversal in the measurement domain is not expected, due to the low amplitude and shallow aspect ratio of the roughness.

SPATIAL STRUCTURE OF TURBULENCE QUANTITIES

The collected data from the hot-wire anemometer are a number of time series of streamwise velocity, with each time series corresponding to a particular location in space. At each of these locations, the time series $u(t)$ can be decomposed into a mean component $\bar{u}$ and a zero-mean fluctuating component u', as in Equations 4 and 5.

$$\bar{u}(x,y,z) = \frac{\int_0^\tau u\,dt}{\tau} \qquad (4)$$

$$u'(x,y,z,t) = u(x,y,z,t) - \bar{u}(x,y,z) \qquad (5)$$

Data from different series taken at the same y-location while varying the other coordinates x and z can be decomposed into a spatial average over a full wavelength of the roughness $\langle u \rangle$ and a spatial fluctuation $\tilde{u}$, as in Equations 6 and 7. The two decompositions can be combined to give Equation 8.

$$\langle u \rangle(y,t) = \int_0^{\lambda_x} \int_0^{\lambda_z} u(x,y,z,t)\,dz\,dx \qquad (6)$$

$$\bar{u}(x,y,z,t) = u(x,y,z,t) - \langle u \rangle(y,t) \qquad (7)$$

$$u(x,y,z,t) = \langle \bar{u} \rangle(y) + \langle u' \rangle(y,t) + \tilde{u}(x,y,z) + \tilde{u}'(x,y,z,t) \qquad (8)$$

Because measurements were taken with only a single hot-wire, the two time-varying terms $\langle u' \rangle$ and $\tilde{u}'$ cannot be distinguished and are gathered together as u' in Equation 9, consistent with the definition in Equation 5.

$$u(x,y,z,t) = \langle \bar{u} \rangle(y) + \tilde{u}(x,y,z) + u'(x,y,z,t) \qquad (9)$$

A field quantity $Q(x,y,z)$ which varies in the periodic directions x and z can be transformed by applying a Fourier transform in x and a cosine transform (to enforce symmetry) in z to yield the spatial Fourier mode $\widehat{Q}(y,k,m)$ with streamwise wavenumber k and spanwise wavenumber m, defined in Equation 10.

$$\widehat{Q}(y,k,m) = \int_0^{\lambda_x} \int_0^{\lambda_z} e^{-ikx} \cos(mz) Q(x,y,z) dx dz \qquad (10)$$

Time-Averaged Velocity Field

By performing a number of traverses within a single period of roughness, it is possible to map the streamwise and spanwise variation in the time-averaged velocity, $\tilde{u}$. Figure 1 shows the spatial variation in the mean streamwise velocity in the $z = 0$ plane, a streamwise-aligned plane that sits over a crest in the spanwise roughness variation. The position $x/\lambda_x = 0$ corresponds to a peak in the streamwise direction while $x/\lambda_x = 0.5$ corresponds to a trough in the streamwise direction. The pattern is clearly very close to singly-periodic with a wavelength matching the roughness wavelength. Close to the wall, there is a strong velocity deficit located on the rising portion of the peak. Further from the wall, velocity deficits sit over troughs while pockets of excess velocity sit over peaks. Measurable and coherent velocity variation exists throughout the entire boundary layer, with peak amplitude equal to $0.21u_\tau$.

Spatial Fourier Decomposition of Time-Averaged Velocity

The nearly-single-periodicity of the mean velocity variation suggests that a spatial Fourier transform of the velocity field could be useful in decomposing the flow field. Performing a Fourier transform of mean velocity $\bar{u}(x,y,z)$ in x and a cosine transform in z (to ensure spanwise symmetry) yields a set of spatial Fourier modes $\widehat{u}(y,k,m)$, where k is the streamwise wavenumber and m the spanwise wavenumber. Following the Nyquist criterion, one can determine from the four-by-two grid of data modes with $k = 0, k_x$ and $m = 0, k_z$, where k_x and k_z are the streamwise and spanwise roughness wavenumbers, respectively.

The streamwise-varying-only mode $\widehat{u}(y,k_x,0)$ is the strongest mode, as expected from the blockage effect created by spanwise-constant features, and is plotted in Figure 2. The qualitative features of the full mean velocity field are also evident in this mode, with its amplitude peaking near the wall and the high-speed regions over roughness peaks.
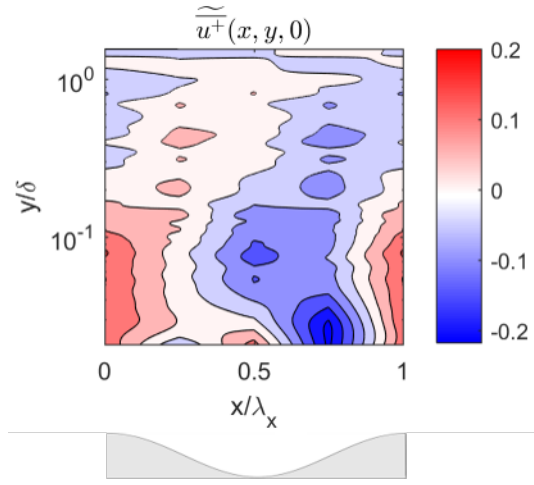

Figure 1: Spatial variation of the inner-normalized mean velocity field $\widetilde{u^+}$ on the $z = 0$ plane. Red contours indicate a region in which the flow is faster than at other points at the same y-location. The position $x/\lambda_x = 0$ corresponds to a peak in the streamwise direction while $x/\lambda_x = 0.5$ corresponds to a trough in the streamwise direction.
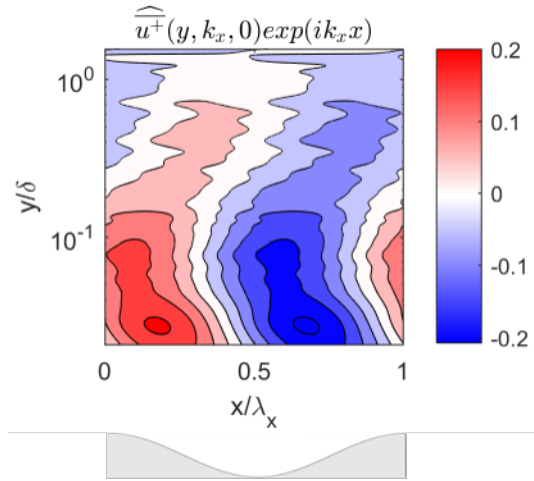

Figure 2: Mean velocity spatial Fourier mode $\widehat{u}(y,k_x,0)$, with red denoting a region of flow which is faster than the streamwise and spanwise mean. The position $x/\lambda_x = 0$ corresponds to a roughness peak in the streamwise direction while $x/\lambda_x = 0.5$ corresponds to a trough in the streamwise direction.

Spatially-Averaged Velocity Power Spectra

The velocity power spectrum, like the mean velocity, can be averaged over a roughness wavelength for comparison to the smooth wall case. At each location (x,y,z) for which there is a velocity trace, the time series is transformed into a spatial velocity series using Taylor's frozen turbulence hypothesis and a convection velocity equal to the spatially- and temporally-averaged velocity at each y-location. A power spectrum is then calculated for each time series as a function of Taylor-transformed wavelength λ_T. Figure 3 plots the spatial-averaged pre-multiplied Taylor-transformed wavelength power series $\langle \lambda_T \Phi(y,\lambda_T) \rangle$ for both smooth wall (filled contours) and rough wall (unfilled contours). In order to filter the noise associated with calculating the power spectrum of a finite time series, a

3   8A-1

moving average filter was applied to the premultiplied power spectrum with a width equal to one tenth of a decade in wavelength. Consistent with the results for velocity variance, the rough wall boundary layer contains less energy than the smooth case at all values of (y, λ_T). This is especially clear away from the roughness wavelength, marked with a red line in the plot.
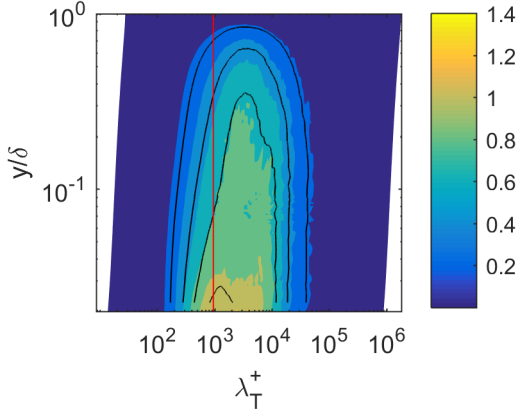

Figure 3: Comparison of spatially-averaged pre-multiplied Taylor wavelength power spectra $\langle \lambda_T \Phi(y, \lambda_T) \rangle$ for rough (unfilled contours) and smooth (filled contours) cases

Spatial Fourier Decomposition of Velocity Power Spectra

Like the mean velocity, the spatial variation in the rough-wall power spectrum can be decomposed into spatial Fourier modes, $\widehat{\lambda_T \Phi}(y, \lambda_T, k, m)$. As for the velocity modes, the streamwise-varying-only mode is the strongest, so the other modes are omitted here. Plotting the magnitude (Figure 4) and phase (Figure 5) over the (y, λ_T) space reveals a strong correspondence between the roughness wavelength (red line) and the magnitude and phase of the mode. The amplitude of the mode has a distinct peak on this red line, indicating that the part of the power spectrum with the most spatial variation is the part of the spectrum corresponding to the roughness wavelength. The phase plot also reveals a strong coherence in phase at that Taylor wavelength.

Isolating the phase and magnitude along the line of $\lambda_T = \lambda_x$ allows the construction of a streamwise-varying-only mode in the same sense as in Figure 2. This mode, plotted in Figure 6, shows the streamwise and wall-normal variation in the velocity power spectrum of the flow at the Taylor wavelength equal to the roughness wavelength. As evident in Figures 4 and 5, the mode is strongest in amplitude near the wall and there are large phase shifts through the boundary layer.

SPATIAL VARIATION OF THE VELOCITY POWER SPECTRUM AND PHASE RELATIONSHIPS IN TRI-ADIC INTERACTIONS

All velocity measurements presented in this paper are taken with a single one-component hotwire probe. Placed at a particular measurement location, the probe produces a time series of the local streamwise velocity. While Taylor's hypothesis can be used to infer from the time series a spatial structure in the velocity field, the inference is not exact. Applying Taylor's hypothesis requires the assumption that all structures in the flow are convecting downstream with at the local mean streamwise velocity. This assumption
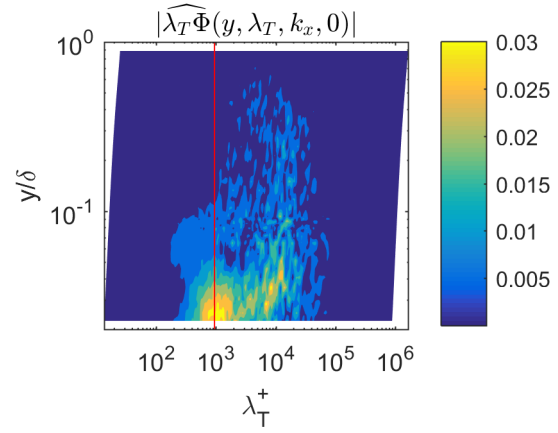

Figure 4: Magnitude of streamwise-varying spatial Fourier mode of the pre-multiplied Taylor wavelength power spectrum $|\widehat{\lambda_T \Phi}(y, \lambda_T, k_x, 0)|$. The red line corresponds to the roughness wavelength
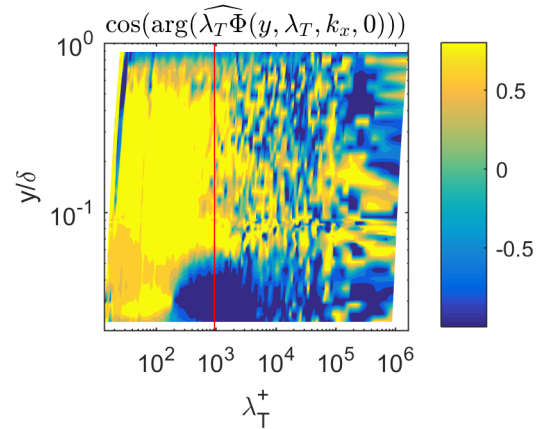

Figure 5: Cosine of the phase of streamwise-varying spatial Fourier mode of the pre-multiplied Taylor wavelength power spectrum $\cos(\arg(\widehat{\lambda_T \Phi}(y, \lambda_T, k_x, 0)))$. The red line corresponds to the roughness wavelength. Zero phase corresponds to a spatial maximum directly above a maximum of roughness height.

of a fixed convection speed creates a one-to-one relationship between spatial wavenumber and time frequency which is not true in general. The true velocity field of a turbulent flow can be Fourier-decomposed into the sum of spatially-varying waves which are periodic in the homogeneous dimensions, with arbitrary combinations of wavenumbers and frequencies. Equation 11 expresses that representation for the case of a flow which varies only in the streamwise coordinate x and time coordinate t. Each component wave has an associated amplitude a_p, spatial wavenumber k_p, phase ϕ_p, and angular frequency ω_p which is defined to be non-negative without loss of generality. The expression can be extended to a three-dimensional boundary layer by including a spanwise homogeneous coordinate z and by allowing the amplitude and phase to vary with the wall-normal coordinate y. These are omitted here for brevity without changing the qualitative result.
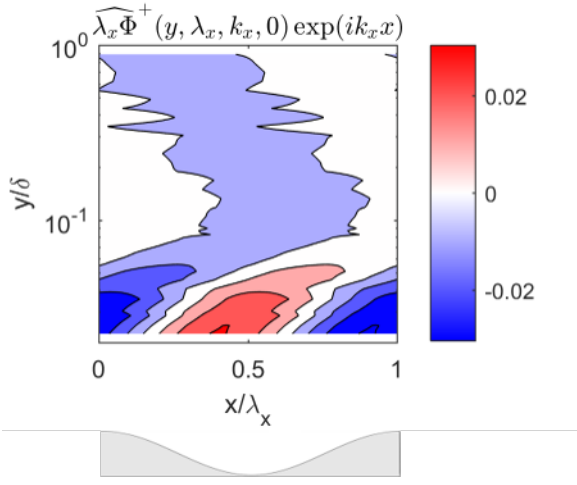
Figure 6: Velocity power spectrum spatial Fourier mode $\widehat{\lambda_x \Phi}^+(y, \lambda_x, k_x, 0)$, with red denoting a region of flow which is more energetic than the streamwise and spanwise mean. The position $x/\lambda_x = 0$ corresponds to a roughness peak in the streamwise direction while $x/\lambda_x = 0.5$ corresponds to a trough in the streamwise direction.

$$u(x,t) = \sum_{p=1}^{\infty} a_p(e^{i(k_p x + \omega_p t + \phi_p)} + e^{-i(k_p x + \omega_p t + \phi_p)}) \quad (11)$$

The Fourier transform in time of $u(x,t)$ is defined to be $\mathcal{U}(x,\omega)$ in Equation 12 and can be evaluated as Equation 13 after applying the restriction that $\omega_p, \omega \geq 0$.

$$\mathcal{U}(x,\omega) = \overline{e^{-i\omega t} \sum_{p=1}^{\infty} a_p(e^{i(k_p x + \omega_p t + \phi_p)} + e^{-i(k_p x + \omega_p t + \phi_p)})} \quad (12)$$

$$\mathcal{U}(x,\omega) = \sum_{\substack{p=1 \\ \omega=\omega_p}}^{\infty} a_p e^{i(k_p x + \phi_p)} \quad (13)$$

The velocity power spectrum in time $\Phi(x,\omega)$ of such a flow is the energy associated with a particular angular frequency ω, defined in Equation 14. Expanding the multiplication then results in Equation 15, which is an expression of the power spectrum as a double summation.

$$\Phi(x,\omega) = |\mathcal{U}(x,\omega)|^2 = \left(\sum_{\substack{p=1 \\ \omega=\omega_p}}^{\infty} a_p e^{i(k_p x + \phi_p)}\right)\left(\sum_{\substack{q=1 \\ \omega=\omega_q}}^{\infty} a_q e^{i(k_q x + \phi_q)}\right)^* \quad (14)$$

$$\Phi(x,\omega) = \sum_{\substack{p=1 \\ \omega=\omega_p}}^{\infty} \sum_{\substack{q=1 \\ \omega=\omega_q}}^{\infty} a_p a_q e^{i((k_p - k_q)x + \phi_p - \phi_q)} \quad (15)$$

Further taking the spatial Fourier transform of the power spectrum in x removes the x-dependence of the expression, resulting in a double summation, Equation 16, with conditions that resemble the constraints on non-linear triadic interactions in turbulent flow.

$$\widehat{\Phi}(k,\omega) = \sum_{\substack{p=1 \\ \omega=\omega_p}}^{\infty} \sum_{\substack{q=1 \\ \omega=\omega_q \\ k_q=k_p\pm k}}^{\infty} a_p a_q e^{i(\phi_p - \phi_q)} \quad (16)$$

In fact, the conditions of the summation for the case of $k = k_x$ (as in Figure 4) amount to $\omega_p - \omega_q = 0$ and $k_p - k_q = \pm k_x$, exactly the conditions for pairs of modes to be triadically consistent with the roughness-associated stationary Fourier mode of mean velocity in Figure 2.

The streamwise spatial Fourier modes of mean velocity and power spectral density (plotted in Figures 2 and 6) each have an associated phase, defined as the spatial phase difference in the x-direction between the maximum of the Fourier mode and the roughness peak. The variation of this phase in y is plotted in Figure 7. Notably, the two fields are nearly anti-correlated close to the wall and on the edge of the boundary layer, while they are nearly perfectly correlated in a layer of intermediate y. This behavior is opposite to that of the Ψ of Duvvuri et al.
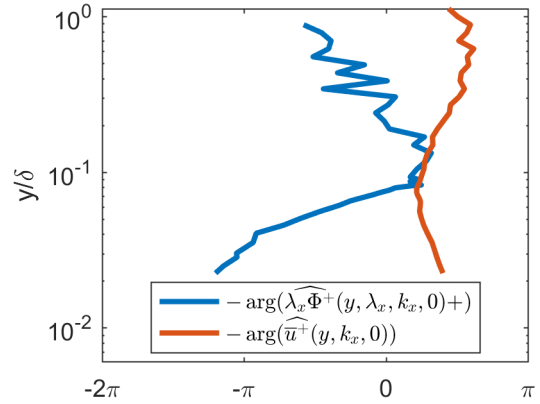

Figure 7: Phases of stationary roughness velocity mode $\widehat{u}(y, k_x, 0)$ and power spectrum at roughness wavelength $\widehat{\lambda_x \Phi}(y, \lambda_x, k_x, 0)$. A phase of zero means that a local maximum of the spatial field is directly above a local maximum of roughness height. The negative phase is plotted here so that a negative value on the horizontal axis corresponds to an upstream (leftward) shift.

Taking Ψ as inspiration, one can define a power spectrum correlation coefficient which correlates the static roughness velocity mode $\widehat{u}(y, k_x, 0) \exp(ik_x x)$ with the power spectrum at roughness wavelength $\widehat{\lambda_T \Phi}(y, \lambda_x, k_x, 0) \exp(ik_x x)$. As these modes are both sinusoidal in x, their correlation may be represented simply as in Equation 17. The correlation coefficient Ξ is similar to the cospectral density of Jacobi & McKeon (2013), with both quantities relating velocity fluctuations at particular scales. In contrast to the cospectral density, the coefficient Ξ considers a single scale for the small-scale fluctuations (with a fixed λ) in addition to a fixed scale for the overlying disturbance.

$$\Xi = \cos(\arg(\widehat{\lambda_T \Phi}(y,\lambda_x,k_x,0)) - arg(\widehat{u}(y,k_x,0))) \qquad (17)$$

The result is plotted in Figure 8. The behavior away from the wall is nearly the opposite of Ψ, hinting at a connection between the two phenomena. The phase shifts in Ψ have been interpreted in the context of critical layers of the synthetic mode, but the roughness mode here has no velocity and therefore no critical layer. This may explain the deviation near the wall, where Ξ sharply transitions from some positive value to -1.
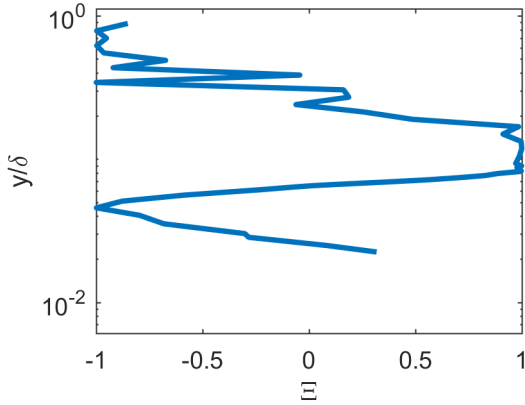

Figure 8: Power Spectrum Correlation Coefficient Ξ

Implications for Real-World Roughness

Equation 16 allows a striking interpretation of Figures 4 and 5: the stationary, spatially periodic mean velocity field induced by a static, periodic roughness has an organizing effect on pairs of triadically-consistent spatio-temporal Fourier modes in the flow. These pairs of non-stationary modes which are triadically consistent with the roughness are most clearly organized at frequencies which correspond (through Taylor-transformation) to the roughness wavelength. Because the pairs of spatio-temporal Fourier modes must have non-zero frequency to show up in the power spectrum, and the roughness-associated mean velocity field must be static with zero frequency, the interactions which connect them must be non-linear. The large horizontal and vertical length scales introduced by the the roughness into the flow allow a single hotwire probe to map these non-linear interactions.

The turbulent boundary layer examined here differs from a canonical smooth-wall boundary layer due to a perturbation of the wall boundary condition by a small-amplitude roughness. The roughness then creates, through a nominally linear boundary condition, a stationary variation in the mean velocity field which does not exist in the canonical flow. This stationary field interacts non-linearly with the broad spectrum characteristic of wall-bounded turbulence, organizing pairs of triadically-consistent modes in a coher-

ent manner. Thus altered, the spatio-temporal modes interact non-linearly with each other to produce a field of Reynolds stress which is different from the smooth-wall case, affecting the mean profile and therefore important parameters such as the friction coefficient.

On a typical real-world surface, many roughness length scales would be present. Many of these length scales would also likely be much smaller than the boundary layer thickness, limiting their influence to a small region of the flow. If, however, a few dynamically-important scales can be isolated, their linear effects computed and superposed, and their non-linear effects on the turbulent spectrum accurately modeled, it may be possible to predict the effect of an arbitrary roughness on a boundary layer.

CONCLUSIONS

A singly-periodic roughness with a length scale on the order of the boundary layer thickness was introduced to a turbulent boundary layer. This large length scale created an inhomogeneous mean velocity field, fixed to the roughness and persisting through the whole boundary layer. The mean velocity field was shown, through the spatial variation in the power spectrum, to have a phase-organizing effect on triadically-consistent traveling waves, with the strongest effects corresponding to waves with a Taylor wavelength similar to the roughness wavelength. The introduction of a single large scale has allowed us to trace the effect of a single mode of roughness from the linear boundary conditions of the roughness through to the resulting non-linear interactions. An extension of this analysis, applied to the dynamically important scales of a real roughness, may be able to predict the effects of the roughness on the physics of the turbulent boundary layer.

ACKNOWLEDGEMENTS

REFERENCES

Bandyopadhyay, PR & Hussain, AKMF 1984 The coupling between scales in shear flows. *Phys. Fluids* **27** (9), 2221–2228.

De Graaff, DB & Eaton, JK 2000 Reynolds-number scaling of the flat-plate turbulent boundary layer. *J. Fluid Mech.* **422**, 319–346.

Duvvuri, S & McKeon, BJ 2015 Triadic scale interactions in a turbulent boundary layer. *J. Fluid Mech.* **767**, R4.

Flack, KA & Schultz, MP 2014 Roughness effects on wall-bounded turbulent flows. *Phys. Fluids (1994-present)* **26** (10), 101305.

Jacobi, I & McKeon, BJ 2013 Phase relationships between large and small scales in the turbulent boundary layer. *Exp. Fluids* **54** (3), 1481.

MacDonald, M, Chung, D, Hutchins, N, Chan, L, Ooi, A & García-Mayoral, R 2016 The minimal channel: a fast and direct method for characterising roughness. In *J. of Phys.: Conf. Series*, , vol. 708, p. 012010. IOP Publishing.

Mathis, R, Hutchins, N & Marusic, I 2009 Large-scale amplitude modulation of the small-scale structures in turbulent boundary layers. *J. Fluid Mech.* **628**, 311–337.

Mejia-Alvarez, R & Christensen, KT 2010 Low-order representations of irregular surface roughness and their impact on a turbulent boundary layer. *Phys. Fluids (1994-present)* **22** (1), 015106.